The Astrophysical Journal, 973:93 (9pp), 2024 October 1 https://doi.org/10.3847/1538-4357/ad66d0

Revised Reaction Rate for the Astrophysical Reaction $^{18}O(p, \alpha)^{15}N$ via a Global *R*-matrix Analysis

Yi-Yang Li[1,2], Jun Hu[1,2,4], Long-Hui Ru[1,4], Ning Tian[1,2,3], and Jin-Feng Lv[3]
[1] Institute of Modern Physics, Chinese Academy of Sciences, Lanzhou 730000, People's Republic of China; hujunbaggio@impcas.ac.cn, rulonghui@impcas.ac.cn
[2] School of Nuclear Science and Technology, University of Chinese Academy of Sciences, Beijing 100049, People's Republic of China
[3] School of Nuclear Science and Technology, Lanzhou University, Lanzhou 730000, People's Republic of China
Received 2023 August 29; revised 2024 July 15; accepted 2024 July 22; published 2024 September 23

Abstract

The $^{18}O(p, \alpha)^{15}N$ reaction is of particular importance for influencing the abundances of key isotopes such as ^{19}F, ^{18}O, and ^{15}N. Peculiar abundances for these nuclei are observed from spectra or meteorite grains originating in asymptotic giant branch stars. The $^{18}O(p, \alpha)^{15}N$ could provide a way to explain the discrepancy between the observations and model predictions. A comprehensive *R*-matrix analysis has been performed for the $^{18}O(p, \alpha)^{15}N$ reaction by including additional constraints from other reaction channels; in particular, the $^{15}N+\alpha$ scattering data were involved in the analysis for the first time. All available data were compiled and used in the *R*-matrix analysis. The fitted resonance parameters are compared with previous works. A revised determination of reaction rate has been extracted, relying on the present fitting parameters. The uncertainties on the corresponding reaction rates were then obtained by a Monte Carlo analysis.

Unified Astronomy Thesaurus concepts: Nuclear reaction cross sections (2087); Reaction rates (2081); Stellar nucleosynthesis (1616)

1. Introduction

In certain astrophysical environments, the $^{18}O(p, \alpha)^{15}N$ reaction has been demonstrated to play a pivotal role as it influences the production of important isotopes such as ^{19}F, ^{18}O, and ^{15}N. These isotopes can be utilized to probe various astrophysical scenarios and test currently accepted models. In particular, spectroscopic observations indicated a significant enhancement in the abundance of fluorine in asymptotic giant branch (AGB) stars compared to its solar abundance (Jorissen et al. 1992). The ^{19}F is generated in the helium intershell of AGB stars and subsequently dredged up to the stellar surface along with *s*-process elements (Lugaro et al. 2004). The $^{18}O(p, \alpha)^{15}N$ reaction could provide a way to explain the issue of ^{19}F abundance. It can affect fluorine yield from AGB stars since it produces ^{15}N nuclei, which are later burned to ^{19}F through the $^{15}N(\alpha, \gamma)^{19}F$ capture reaction during a thermal pulse. As a result, a larger $^{18}O(p, \alpha)^{15}N$ reaction rate would lead to an increase of ^{19}F supply, alleviating the discrepancy between the observations and model predictions. Meanwhile, an enrichment of ^{15}N in the stellar surface could play a key role to explain the long-standing problem of the extremely small $^{14}N/^{15}N$ ratio in meteorite grains (Nollett et al. 2003). Furthermore, peculiar $^{18}O/^{16}O$ ratios are observed in oxygen-rich Group II grains originating in intermediate-mass AGB stars, showing significantly higher values than those predicted by models (Lugaro et al. 2017). The $^{18}O(p, \alpha)^{15}N$ is the primary destructive reaction for the ^{18}O abundance. Thus, a revised $^{18}O(p, \alpha)^{15}N$ reaction rate might provide a clue to better understand the $^{18}O/^{16}O$ ratio problem.

The $^{18}O(p, \alpha)^{15}N$ reaction has been investigated over a wide range of beam energies via both direct (Mak et al. 1978; Lorenz-Wirzba et al. 1979; Bruno et al. 2019) and indirect (La Cognata et al. 2008) measurements. The $1/2^+$ resonances at $E_x = 8.138$, 8.650, and 8.793 MeV (see Figure 1) contribute the most to the reaction rates at temperatures of astrophysical interest ($T = 0.01$–1.00 GK). The narrow resonance at $E_x = 8.138$ MeV is fairly well established. The broad resonance at $E_x = 8.650$ MeV gives strong contributions both at low and high temperatures. The most recent measurement for this resonance was carried out by La Cognata et al. (2010). Later on, revised level parameters for the $E_x = 8.650$ MeV state were obtained by Bruno et al. (2019) via an *R*-matrix reanalysis combining their low-energy $^{18}O(p, \alpha)^{15}N$ data and high-energy data from Lorenz-Wirzba et al. (1979). By far, results on its level properties are largely inconsistent. Its resonance energy, $E_r = 590 \sim 658$ keV, is quite uncertain, and the α width Γ_α is also poorly known, ranging from 90 to 320 keV in different studies (Yagi 1962; Mak et al. 1978; Lorenz-Wirzba et al. 1979; La Cognata et al. 2008, 2010; Bruno et al. 2019). The other broad resonance at $E_x = 8.793$ keV contributes significantly at high temperatures. Results on its resonance parameters are quite consistent in several measurements (Yagi 1962; Mak et al. 1978; Lorenz-Wirzba et al. 1979) as well as an *R*-matrix reanalysis by Bruno et al. (2019), except that a 10 keV difference of E_r was reported by Christensen et al. (1990) and La Cognata et al. (2010), and a 20 keV higher Γ_α was also yielded by La Cognata et al.'s *R*-matrix analysis (La Cognata et al. 2010). In addition, a broad $1/2^-$ resonance at higher energy was introduced as a background state in the *R*-matrix analysis of Mak et al. (1978) and Bruno et al. (2019). This state would interfere with the last two $1/2^+$ levels and significantly impact the excitation function curve. Although the cross section has been measured directly to energies as low as $E_{c.m.} = 55$ keV (Bruno et al. 2019), significant uncertainties remain that affect the extrapolation of $S(0)$ factor. Consequently, the stellar reaction rate is still with a large uncertainty.

[4] Corresponding author.

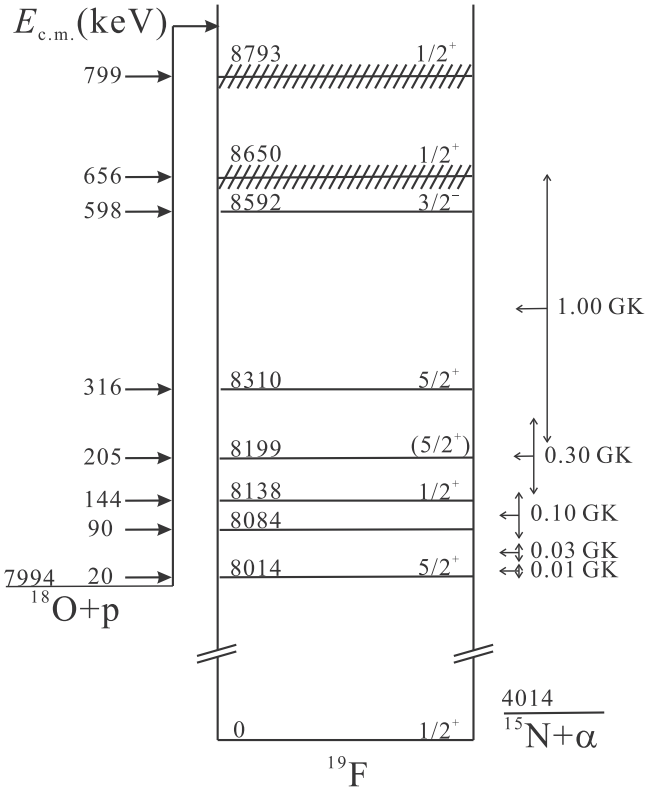

Figure 1. Energy level diagram of ^{19}F. The levels with shaded area are the broad resonances. The level properties are taken from Tilley et al. (1995).

In the present paper, we perform a new global *R*-matrix analysis for the ^{18}O(p, α)^{15}N reaction by involving the ^{15}N(α, α)^{15}N data for the first time. The *S*-factor is extrapolated to the energies of astrophysical interest, and an improved reaction rate is extracted based on the fitting resonance parameters. The details of the analysis are described in Section 2. The revised $S(0)$ factor and its uncertainty estimation are presented in Section 3. An updated reaction rate and comparison with previous works are depicted in Section 4. Finally, this work is summarized in Section 5.

2. *R*-matrix Analysis

The *R*-matrix formalism is a crucial tool in the study of nuclear astrophysics reactions. The introduction of *R*-matrix theory allows for more reliable interpretation of the observed experimental data since it makes it possible to accurately account for interference effects between multiple resonant and nonresonant contributions.

A multichannel, multilevel *R*-matrix code AZURE2 (Azuma et al. 2010) was used for the analysis. Initial values for resonance energies, widths, and spin-parities are taken from Tilley et al. (1995). These values often provide a good starting point for the *R*-matrix fit. Cross sections, *S*-factors, and particle partial widths throughout this work are always in the center-of-mass system. In the present *R*-matrix analysis, more available data from other reaction channels are considered to provide additional constraints. Since the γ branches are expected to be weak, the γ channels are neglected in the analysis. The *R*-matrix calculation is also done in the Brune parameterization (Brune 2002), allowing for the direct use of observable level energies and widths.

The proton and α channels are considered in the analysis. The channel radii are taken to be $R_p = 5.1$ fm for the proton channel and $R_\alpha = 5.7$ fm for the α channel, as calculated from the equation $1.4 \times (A^{1/3}_{^1\mathrm{H}(^4\mathrm{He})} + A^{1/3}_{^{18}\mathrm{O}(^{15}\mathrm{N})})$. Both values are the same with those of Yagi (1962) and Mak et al. (1978). Bruno et al. (2019) set both channel radii to be 5 fm and found no significant differences using 5.5 or 6 fm. $R_p = 4.71$ fm and $R_\alpha = 5.27$ fm were adopted by La Cognata et al. (2019) using the same equation as us but selecting the $r_0 = 1.3$ fm. A test of channel radii dependence for the *R*-matrix analysis was carried out using the radii values mentioned above. No significant difference was observed, and our choice was found to better describe the data.

The separation energies for proton and α are 7.994 MeV and 4.014 MeV, respectively. The following subsections detail the different reaction channels included in this analysis. Although they are described individually, the fits to the different particle-reaction-channel data sets have been performed simultaneously.

For the following *R*-matrix fitting plots, center-of-mass energy is given on the bottom horizontal axis and the excitation energy on the top horizontal axis of the plot. The fitted resonance parameters relevant to the astrophysical reaction ^{18}O(p, α)^{15}N are listed in Table 1. Since we implemented the first global *R*-matrix analysis by involving the ^{15}N+α elastic scattering data (La Cognata et al. 2019), much more levels were taken into account in the present analysis. Table 2 lists all the levels' properties obtained in our global *R*-matrix analysis.

2.1. ^{18}O(p, α)^{15}N

Mak et al. (1978) measured the total cross section of ^{18}O(p, α)^{15}N over the energy range 223 keV $< E_{c.m.} <$ 661 keV. An $S(0)$ factor was extrapolated to be 46 MeV b using the *R*-matrix theory. Lorenz-Wirzba et al. (1979) investigated the differential cross sections in the energy range $E_{c.m.} = 68$–886 keV at $\theta_{lab} = 135°$ and 90°, respectively. With the use of high-beam currents, they confirmed the three known resonances above $E_{c.m.} = 587$ keV and observed four new resonances below $E_{c.m.} = 322$ keV. Recently, Bruno et al. (2019) performed the most updated direct measurement of the differential cross section at $\theta_{lab} = 135°$ and 102.°5 from $E_{c.m.} = 340$ keV down to $E_{c.m.} = 55$ keV. This experiment was carried out at the Laboratory for Underground Nuclear Astrophysics with the lowest energy measured by far.

These three measurements reviewed here are the most recent reported ones for astrophysical application. Thus, in the present analysis, we included the angle-integrated cross sections from Mak et al. (1978; data for Figure 4 obtained from EXFOR Zerkin 2019), the differential cross sections at $\theta_{lab} = 135°$ and 90° from Lorenz-Wirzba et al. (1979; digitized from Figure 6), and the differential cross sections at $\theta_{lab} = 135°$ and 102.°5 (Bruno et al. 2019; provided by the author C. G. Bruno). Furthermore, the data from Christensen et al. (1990; data for Figures 2 and 4 obtained from EXFOR Zerkin 2019) were involved as well for providing more constraints on the fit in the specific energy region.

Bruno et al. (2019) performed the first global *R*-matrix analysis by involving the most recent (p, α) and (p, p) data (Mak et al. 1978; Lorenz-Wirzba et al. 1979; Christensen et al. 1990; Bruno et al. 2019). Bruno et al. tried to include the ^{15}N+α elastic scattering data from Smotrich et al. (1961) in their *R*-matrix fit but failed, probably because of the poor energy resolution. Their ^{18}O(p, α)^{15}N data points partly

Table 1
The Level Properties Relevant to the $^{18}O(p, \alpha)^{15}N$ from the Present *R*-matrix Fit, Compared with Previous Works

	Present Work			Bruno et al. (2019)			La Cognata et al. (2010)		
J^π	E_x	Γ_p	Γ_α	E_x	Γ_p	Γ_α	E_x	Γ_p	Γ_α
$3/2^+$	**8.0830(3)**	**7.97(57) × 10^{-10}**	0.155(51)	8.0830(2)	**7.97(57) × 10^{-10}**	0.121(5)	…	…	…
$(1/2^-)$	…	…	…	8.100(3)	1.2(1) ×10^{-7}	86.0(16)	…	…	
$1/2^+$	**8.1368(3)**	**1.64(12) × 10^{-4}**	**0.151(1)**	**8.1368(3)**	**1.64(12) × 10^{-4}**	0.150(1)	…	…	…
$5/2^+$	8.1965(1)	**7.08(56) × 10^{-7}**	**0.012(1)**	**8.1987(3)**	**7.91(56) × 10^{-7}**	0.012(1)	…	…	…
$5/2^+$	**8.3112(3)**	**2.82(20) × 10^{-5}**	**1.9(1)**	**8.3112(3)**	**2.82(20) × 10^{-5}**	1.9(1)	…	…	…
$3/2^-$	8.5872(2)	**0.109**	**2.04**	8.5916(3)	0.036(2)	2.5(1)	…	…	…
$1/2^+$	8.6045(30)	5.72(23)	−149(4)	8.6065(12)	7.7 (1)	163(1)	8.603(2)	11.1(11)	188 (3)
$1/2^+$	8.7920(4)	**29.64**	**29.69**	8.7938(3)	24.4(3)	26.1(3)	8.8065(15)	27 (10)	40^{+5}_{-13}
$3/2^-$	**8.928**	**0.209**	6.52(184)	…	…	…	…	…	…
$7/2^+$	9.1016(7)	**−0.011**	**0.919**	…	…	…	…	…	…
$1/2^+$	9.1681(7)	−0.57(17)	−7.05(252)	…	…	…	…	…	…
$1/2^+$	9.3226(6)	0.232(83)	3.73(167)	…	…	…	…	…	…
		Lorenz-Wirzba et al. (1979)			Mak et al. (1978)			Yagi (1962)	
$3/2^+$	8.083(4)	$\Gamma_{tot} \leqslant 2.8$	…	…	…	…	…	…	…
$1/2^+$	8.137(2)	$\Gamma_{tot} \leqslant 0.47$	…	…	…	…	…	…	…
$5/2^+$	8.198(2)	$\Gamma_{tot} \leqslant 0.95$	…	…	…	…	…	…	…
$5/2^+$	8.309(2)	$\Gamma_{tot} \leqslant 0.95$	…	…	…	…	…	…	…
$3/2^-$	8.589(3)	$\Gamma_{tot} \leqslant 2.8$	…	8.590	0.062[a]	1.9[a]	8.5933(4)	0.062(6)	1.9(2)
$1/2^+$	8.652	6.6	317	8.610	5.5	160	8.638	4.7	90
$1/2^+$	8.795	24.6(15)[a]	19.9(10)[a]	8.795	24.6(15)[a]	19.9(10)[a]	8.7955(15)	24.6(15)	19.9(10)
$3/2^-$	…	…	…	…	…	…	8.9291(7)	0.076 (7)	3.5 (3)
$7/2^+$	…	…	…	…	…	…	9.1010(5)	0.0047 (6)	0.56(8)
$1/2^+$	…	…	…	…	…	…	9.1668(10)	0.38 (3)	5.4(4)
$1/2^+$	…	…	…	…	…	…	9.3227(10)	0.22(2)	4.7(4)
BG[b]		Present Work			Mak et al. (1978)			Bruno et al. (2019)	
$1/2^-$	**25**	2.35(24) × 10^4	1.583(96) × 10^5	8.705	3.2	1060	14.994	2.9(12) × 10^4	4.31(180) × 10^5
$1/2^+$	**25**	−1.85(28) × 10^4	1.16 × 10^3	…	…	…	…	…	…
$3/2^-$	**25**	−9.61 × 10^3	7.84(509) × 10^3	…	…	…	…	…	…
$3/2^+$	**25**	4.00(17) × 10^5	−2.83(12) × 10^5	…	…	…	…	…	…
$5/2^-$	**25**	−1.276(2) × 10^5	4.65	…	…	…	…	…	…
$5/2^+$	**25**	−2.96(22) × 10^5	6.21(46) × 10^5	…	…	…	…	…	…

Notes. Minus signs on the partial widths correspond to the sign of the corresponding reduced width amplitude. The fixed parameters during the fitting are displayed in bold. E_x is in units of MeV; particle widths are in units of keV. The comparison for the background states are listed in the bottom zone of this table.
[a] Taken from Yagi (1962).
[b] Background state.

Table 2
All the Levels Introduced in the Present *R*-matrix Fit, Compared with La Cognata et al.'s Fitted Parameters (La Cognata et al. 2019)

La Cognata et al. (2019)				Present Work			
J^π	E_x	Γ_p	Γ_α	$J^{\pi a}$	E_x	Γ_p	Γ_α
$7/2^+$	7.114	⋯	18.6	⋯	7.1239	⋯	18.76
$5/2^+$	7.364	⋯	99.9	⋯	7.3453	⋯	98.57
$7/2^+$	7.56	⋯	158	⋯	**7.56**	⋯	127.68
$1/2^-$	7.702	⋯	327	⋯	7.7675	⋯	99.0
$5/2^-$	7.74	⋯	73.7	⋯	7.6913	⋯	128.03
$7/2^+$	7.929	⋯	263	⋯	7.9025	⋯	155.97
$11/2^+$	7.937	⋯	–[b]	⋯	**7.937**	⋯	1.42×10^{-10}
$1/2^+$	7.979	⋯	1.10	⋯	**7.9**	⋯	**28.2**
$5/2^+$	8.014	0	0	⋯	⋯	⋯	⋯
$9/2^-$	8.084	0	8.06	$3/2^+$	**8.083**	$\mathbf{7.97 \times 10^{-10}}$	0.155
$1/2^+$	8.1377	–[b]	1008	⋯	**8.1368**	$\mathbf{1.64 \times 10^{-4}}$	0.151
$11/2^+$	8.1384	0	22.2	⋯	8.1258	⋯	57.18
$5/2^+$	8.199	–[b]	35.9	⋯	8.1965	$\mathbf{-7.08 \times 10^{-7}}$	**−0.012**
$13/2^-$	8.288	0	2.14	⋯	8.2873	⋯	1.89
$5/2^+$	8.310	–[b]	3.59	⋯	**8.3112**	$\mathbf{2.82 \times 10^{-5}}$	**1.9**
$7/2^+$	8.3745	0	10.9	⋯	**8.445**	⋯	**230.1**
$3/2^-$	8.5919	–[b]	659	⋯	8.5872	**0.11**	**2.04**
$1/2^+$	8.4585	12.9	87.8	⋯	8.6045	5.7	−148.54
	⋯	⋯	⋯	$5/2^-$	8.6578	⋯	68.22
$1/2^+$	8.7932	52.8	0		8.792	**29.64**	**29.69**
	⋯	⋯	⋯	$7/2^+$	8.8736	⋯	212.87
$3/2^-$	8.9267	–[b]	–[b]	⋯	**8.928**	**0.21**	6.52
$7/2^+$	8.9439	0	3.1	⋯	**8.94**	⋯	13.72
$9/2^-$	8.953	0	20.1	⋯	8.9416	⋯	10.05
$7/2^+$	9.101	0	93.6	⋯	9.1016	**−0.011**	**0.92**
$1/2^+$	9.167	–[b]	–[b]	⋯	9.1681	−0.57	−7.05
$1/2^+$	9.321	922	363	⋯	9.3226	0.23	3.73

Notes. Minus signs on the partial widths correspond to the sign of the corresponding reduced width amplitude. The fixed parameters during the fitting are displayed in bold. E_x is in unit of MeV; particle widths are in units of keV.
[a] J^π only shown for the states with different values of La Cognata et al. (2019).
[b] Not appreciable with La Cognata et al. (2019)'s experiment resolution.

overlapped with those of Lorenz-Wirzba et al. (1979), and a disagreement was found below $E_{\rm c.m.} = 170$ keV. Therefore they discarded these data of Lorenz-Wirzba et al. We would not like to show a preference of one data set over another; hence, our differential cross section data at $\theta_{\rm lab} = 135°$ are combined with both the data from Bruno et al. (2019) and Lorenz-Wirzba et al. (1979).

Mak et al. (1978) introduced a broad $1/2^-$ level as a background state at $E_x = 8.705$ MeV to approximate the $1/2^-$ strength in the region of interest. However, in principle, the background state is a nonphysical state and should be placed far from the investigated region. Similarly, Bruno et al. (2019) also added a background state at $E_x \sim 15$ MeV with $J^\pi = 1/2^-$ in their *R*-matrix fit. In AZURE2, for the correct computation of Coulomb contributions, background states for each wave should be included; otherwise, there is a computational mistake. In the present *R*-matrix analysis, all the possible contributive J^π values (from $1/2^\pm$ to $5/2^\pm$) were considered as the background poles. Contributions from the higher spins were found to be negligible. Meanwhile, the energy dependence of the background pole was tested to select the optimal E_x value. A misplaced background state could have an uncontrollable effect on the astrophysical energy region, devoid of any physical sense, being an artifact to get a better agreement. Finally, the background pole was chosen at $E_x = 25$ MeV as it gave a better fitting curve and a smaller χ^2.

The *R*-matrix fitting curves for ^{18}O(p, α)^{15}N are shown in Figure 2 and Figure 3. Please note the unit for total *S*-factor of Figure 2(d) is shown on the right vertical axis.

It is clear that the 102.°5 data are being missed by the *R*-matrix fit at low energies and to a lesser extent for the 90° data. To solve this problem, we tried to introduce a new state. However, a reasonable fit cannot be achieved even we tested all possible states with different spin-parities. Generally, low-energy data have large error bars, which are larger than data at higher energies, so a weighted fitting procedure tends to fit them poorly by construction. Moreover, low-energy data are often affected by large systematic errors, often not well understood and underestimated. The low-energy data is so scarce that we cannot make a comparison or assessment for different measurements. Thus, more data at low energies, especially scattering data, would help improve the fit.

In a new paper published by Bruno's collaborators using his data (Ananna et al. 2022), deviation from the fit was observed at the high-energy tail of the $E_x = 8.794$ MeV broad resonance, while a nice fitting of the high-energy regions was shown in La Cognata et al. (2010). The reason for this inconsistency could be the lack of sufficient background states included in the fit.

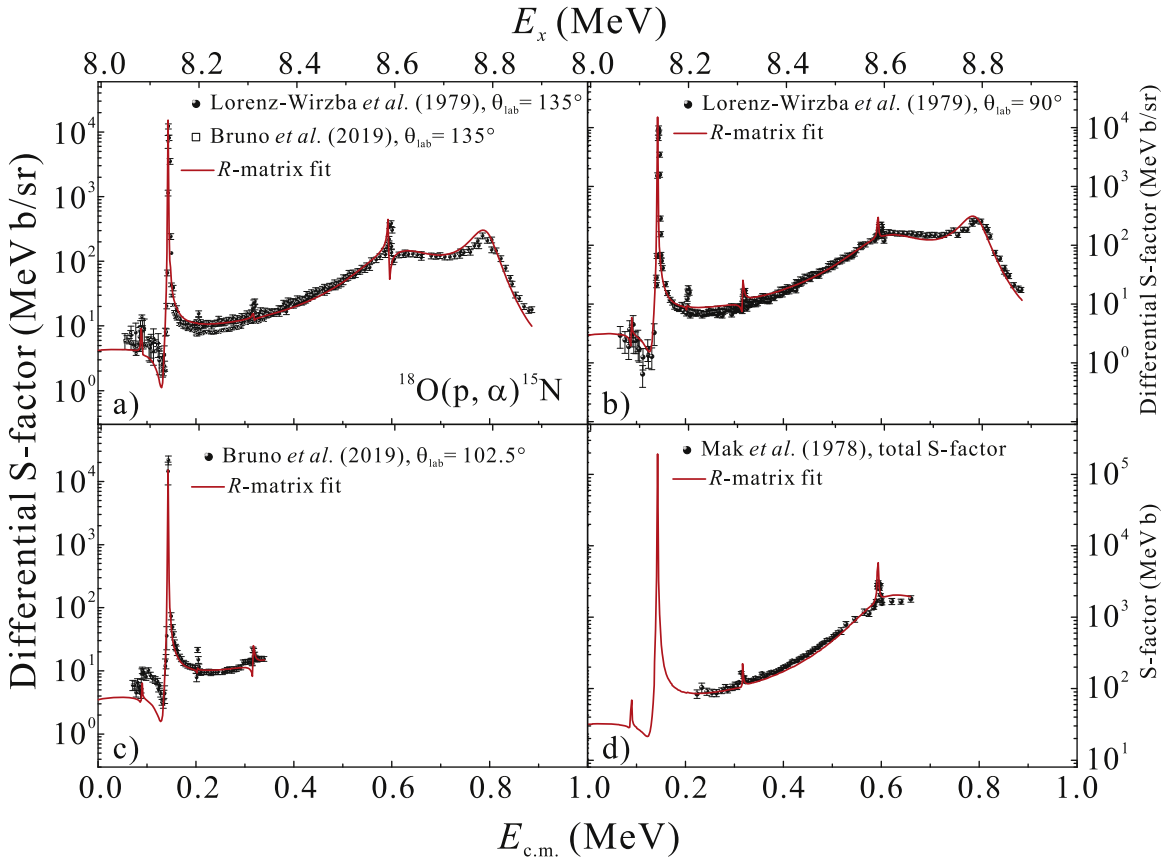

Figure 2. *R*-matrix fits to the ^{18}O(p, α)^{15}N differential cross sections of Bruno et al. (2019) and Lorenz-Wirzba et al. (1979) at $\theta_{lab} = 135°$ (labeled (a)), differential cross sections of Lorenz-Wirzba et al. (1979) at $\theta_{lab} = 90°$ (labeled (b)), differential cross sections of Bruno et al. (2019) at $\theta_{lab} = 90°$ (labeled (c)), and total cross sections of Mak et al. (1978; labeled (d)).

2.2. ^{18}O(p, p)^{18}O

Yagi et al. (1962) performed a precise measurement for the ^{18}O+p elastic scattering and then implemented a careful *R*-matrix analysis for the observed data (Yagi 1962). Two-level approximation to the *R*-matrix was applied to analyze the broad levels of the same spin and parity $1/2^+$, $E_x = 8.638$, and 8.795 MeV resonances. All other weakly excited narrow resonances were analyzed by the one-level approximation and were superposed on the general trend of the excitation curve.

Included in our analysis are the differential cross sections at $\theta_{c.m.} = 140.^{\circ}8$ and 90° from Yagi (1962; data for Figures 5 and 7–11 obtained from EXFOR Zerkin 2019). A 7% uncertainty, estimated by Yagi et al. (1962), was set to these data whose error bar was not available in the EXFOR (Zerkin 2019) database.

The single-channel *R*-matrix analysis performed by Yagi (1962), with no constraints from α channel data, could result in some nonunique or unphysical α widths. For example, a large deviation was found for the Γ_α of $E_x = 8.638$ MeV, $1/2^+$ state compared to our and other fitting results (Mak et al. 1978; Bruno et al. 2019).

The *R*-matrix fitting curves for ^{18}O(p, p)^{18}O are shown in Figure 4.

2.3. $^{15}N(\alpha, \alpha)^{15}N$

Differential cross sections for the elastic scattering of ^{15}N+α were first measured by Smotrich et al. (1961). Almost 60 yr later, Nurmukhanbetova et al. (2017) reported new data of ^{15}N+α elastic scattering at $\theta_{lab} = 0°$ via the Thick Target Inverse Kinematics (TTIK) method. Comparable results were achieved at $E_{c.m.} > 3.0$ MeV compared with the data of Smotrich et al. (1961) at $\theta_{c.m.} = 169.^{\circ}1$.

Most recently, La Cognata et al. (2019) carried out a new ^{15}N+α measurement using the same method that Nurmukhanbetova et al. (2017) performed. They spanned a very large excitation energy range ($E_x \sim 6-10$ MeV) in ^{19}F, which covered the whole energy range of astrophysical interest ($E_x \sim 8-9$ MeV). It might also be noted that the excitation curve of ^{15}N+α elastic scattering is more complicated than that of ^{18}O(p, p)^{18}O and ^{18}O(p, α)^{15}N. More resonant structures appeared in the spectrum, and their level properties are still unknown or uncertain.

La Cognata et al. (2019) performed a simultaneous *R*-matrix fit for their ^{15}N(α, α)^{15}N excitation functions and the ^{18}O(p, p)^{18}O data of Yagi et al. at $\theta_{c.m.} = 140.^{\circ}8$ (Yagi et al. 1962). The general trend was well reproduced, while some small features are not properly reproduced by the fitting. Especially in the energy region of $E_x \sim 8.5-9.0$ MeV, two prominent peak structures showed up, which cannot be reproduced by using known level properties from Tilley et al. (1995). In the present analysis, a good fit can be achieved by introducing two novel states of $E_x = 8.666$ MeV, $5/2^-$ and $E_x = 8.719$ MeV, $3/2^+$. Both states merely have a small impact on the excitation curve of ^{18}O(p, α)^{15}N due to their negligible proton widths.

Included in the analysis are the differential cross sections of La Cognata et al. (2019) at $\theta_{lab} = 0°$, 5°, 10°, and 15° (data for

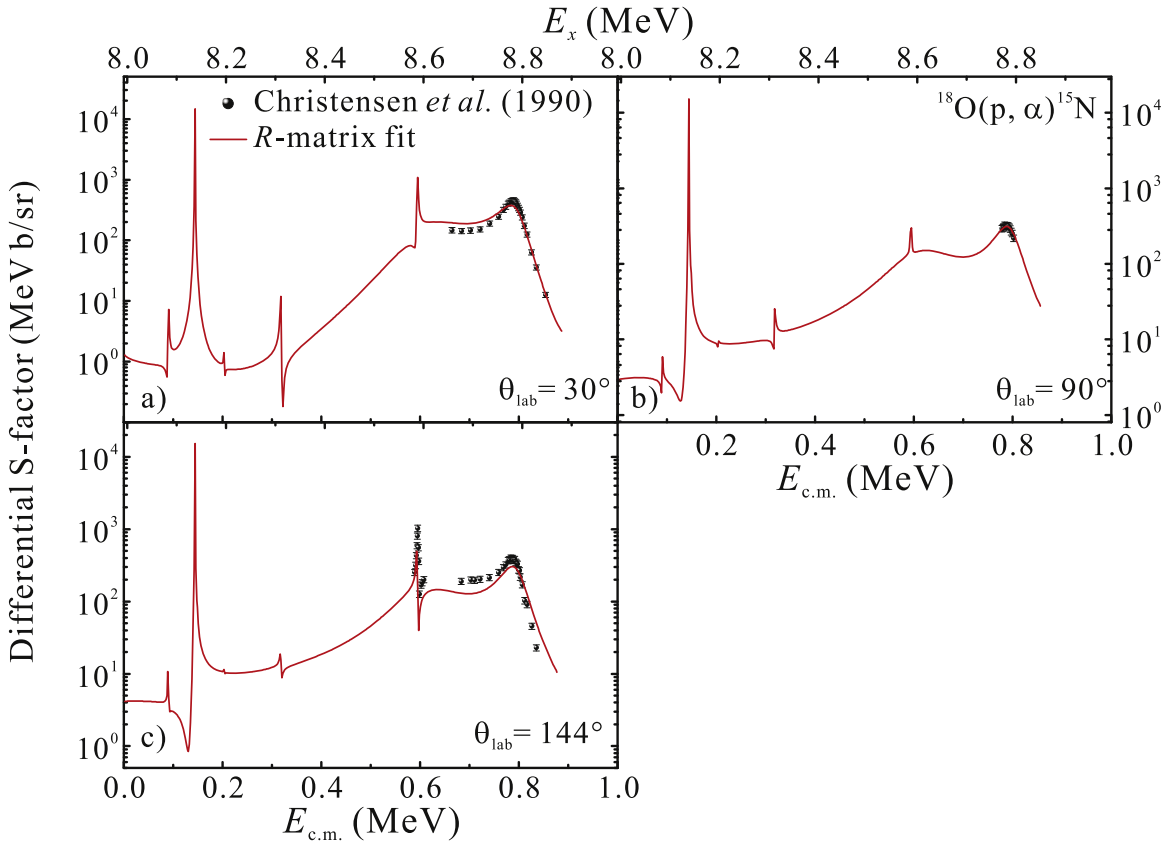

Figure 3. *R*-matrix fits to the ^{18}O(p, α)^{15}N differential cross sections of Christensen et al. (1990) at $\theta_{lab} = 30°$, 90°, and 144° (labeled (a) through (c), respectively).

Figure 2 obtained from EXFOR Zerkin 2019); Nurmukhanbetova et al. (2017) at $\theta_{lab} = 0°$ (data for Figure 6 obtained from EXFOR Zerkin 2019); and Smotrich et al. (1961) at $\theta_{c.m.} = 169.°1$ (data for Figures 4 and 5 obtained from EXFOR Zerkin 2019). Only the data at $E_{c.m.} \sim 3.0-5.0$ MeV were considered in our analysis as the most prominent peak structures appeared in this region. The *R*-matrix fitting curves for ^{15}N(α, α)^{15}N are shown in Figure 5.

Because of the limited energy resolution, the multiple states involved in a broad peak-like structure at $E_{c.m.} \sim 3.76-4.0$ MeV cannot be identified clearly. As a consequence, it was very hard to reproduce the data completely by the fit. A sharp peak lying at $E_{c.m.} \sim 4.0-4.22$ MeV, corresponding to the state of $E_x = 8.123$ MeV, $11/2^+$, agreed with the fit only for the data at $\theta_{lab} = 10°$. In other cases, the fits always overestimated the data near the top region. No explanation for this discrepancy could be found. In the energy region of $E_{c.m.} \sim 4.22-4.55$ MeV, a divergence between the fit and data showed up. This could be attributed to the energy resolution issue and more complicated resonant structure.

2.4. Comparison with Previous Works

It can be seen from Table 1, for the level of $E_x = 8.6045$ MeV, the present fitted excitation energy is in good agreement with the values of Bruno et al. (2019), La Cognata et al. (2010), and Mak et al. (1978). For proton and α widths, they are pretty close to the values reported by Bruno et al. (2019) and Mak et al. (1978), not so different with those of La Cognata et al. (2010). However, large disagreements were found in excitation energy and α width compared with the results of Lorenz-Wirzba et al. (1979) and Yagi (1962).

A very good agreement was found among the different fitting parameters for the other broad $1/2^+$ level at $E_x \sim 8.792$ MeV. A novel state of $E_x = 8.100$ MeV, $1/2^-$ was introduced in the *R*-matrix analysis of Bruno et al. (2019); however, this state did not make any improvement in the present analysis. Therefore, this state was not taken into account in the fit.

Table 2 lists all the the levels introduced in the present global *R*-matrix fit. A comparison has been made with La Cognata et al.'s fitted parameters (La Cognata et al. 2019). Without the constraints from the ^{18}O(p, α)^{15}N data, some level parameters obtained by La Cognata et al. (2019) are quite different from present and previous results (Yagi 1962; Mak et al. 1978; Lorenz-Wirzba et al. 1979; Bruno et al. 2019). For instance, the states of $E_x = 8.1377$, 8.199, and 8.5919 MeV have an overestimated value of Γ_α; the well-known $E_x \sim 8.610$ MeV, $1/2^+$ state was replaced to be at 8.4585 MeV; and unphysical particle widths were given for the $E_x = 9.101$ and 9.321 MeV states as their fit was unable to reproduce these two narrow states from the proton scattering data (Yagi et al. 1962). Low energy resolution data set a poor constraint on the fitting, while high-resolution ones are much more effective, when available. Moreover, the TTIK technique seems to be more sensitive to alpha-cluster states, with small proton partial widths, so some states could be missed in the analysis. It has been demonstrated that a global *R*-matrix analysis, by involving all possible channel data, could provide significant improvement in extracting the level properties.

The $E_x = 8.014$ MeV, $5/2^+$ state, which is of importance at stellar temperatures of $T_9 \lesssim 0.03$ (Lorenz-Wirzba et al. 1979), is also included in the present *R*-matrix fit. Since there are no

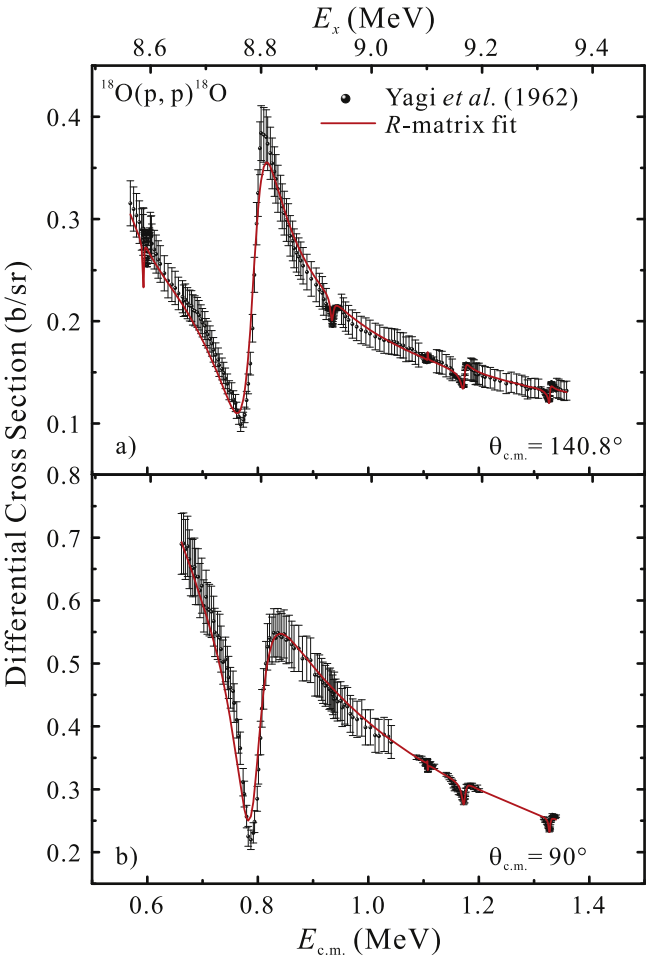

Figure 4. *R*-matrix fits to the ^{18}O(p, p)^{18}O differential cross sections of Yagi (1962) at $\theta_{c.m.} = 140.8°$ and 90°.

available (p, α) and (p, p) data at these energies, constraints from both channels cannot be achieved. This resonance was indeed covered by the ^{15}N(α, α)^{15}N data of La Cognata et al. (2019), Smotrich et al. (1961), and Nurmukhanbetova et al. (2017); however, no clear structure appeared in this region, owing to the energy resolution issue. Thus, the present fit cannot give a firm conclusion for its level properties.

3. Extrapolation of *S*-factor

Because of the exponential behavior of the probability for tunneling, the cross section for charged-particle-induced nuclear reactions drops rapidly for energies below the Coulomb barrier (Rolfs & Rodney 1988). As a consequence, in the typical energy range of stellar burning, the cross sections are extremely low and in most cases cannot be measured directly with available experimental techniques. Cross sections in the stellar energy range are therefore mostly based on extrapolations of existing data from the higher-energy measurements. To make a more reliable extrapolation of the cross sections at low energies, the astrophysical *S*-factor, containing all the strict nuclear effects, was introduced in the nuclear astrophysics community. In addition, the electron screening effect also plays a crucial role at the stellar energies. Since it spoils the low-energy trend of the astrophysical *S*-factor, extrapolation is always necessary.

The *S*-factor for a reaction involving two charged nuclei with atomic numbers Z_1 and Z_2 is defined by (Rolfs & Rodney 1988)

$$S(E) = E\sigma(E)\exp(2\pi\eta), \tag{1}$$

where $\eta = Z_1 Z_2 e^2/(\hbar\upsilon)$ is the Sommerfeld parameter, $\upsilon = \sqrt{2E/\mu}$ the relative velocity of the interacting nuclei, and μ the reduced mass. This definition removes both the $1/E$ dependence of nuclear cross sections and the s-wave Coulomb barrier transmission probability. Thus, *S*-factor is a smoothly varying function of energy and is much more useful in extrapolating measured cross sections to astrophysical energies.

In general, the *S*-factor at low energy is dominated by the nonresonant contribution and more dependent on the background levels. However, in the case of the ^{18}O(p, α)^{15}N reaction, its reaction rate is dominated by several resonances. Even at low temperatures of 0.01–0.012 GK, the rate of $E_r = 20$ keV resonance still plays an overwhelming role. Thus, the extrapolation for the *S*-factor to the stellar energies seems pointless considering the total reaction rate but can give us a better understanding for the nonresonant contributions. An improved $S(0)$ factor of ^{18}O(p, α)^{15}N was determined to be 31.8 ± 1.8 MeV b based on the fitted resonance parameters (see Figure 6). The error was obtained by sampling the fitting parameters with the Monte Carlo method and originated from resonant contribution 0.98 MeV b, nonresonant 1.43 MeV b, and interference effect 0.48 MeV b. Individual contributions of the different background states are also presented in Figure 6. The contribution of $5/2^-$ state is not shown, owing to its small contribution.

4. Reaction Rates

The thermonuclear reaction rates for the ^{18}O(p, α)^{15}N reaction were calculated by numerical integration of the following equation (Rolfs & Rodney 1988):

$$N_A\langle\sigma\nu\rangle = N_A\left(\frac{8}{\pi\mu}\right)^{\frac{1}{2}}\frac{1}{(kT)^{\frac{3}{2}}} \times \int_0^\infty S(E)\exp\left[-\frac{E}{kT} - \left(\frac{E_G}{E}\right)^{1/2}\right]dE, \tag{2}$$

where N_A is Avogadro's number, μ the reduced mass in the entrance channel, k the Boltzmann constant, T the temperature, E_G the Gamow energy, and E the energy in the center of mass. The $S(E)$ in the equation was evaluated from the present fitting level parameters.

There have been several recent investigations of the ^{18}O(p, α)^{15}N reaction rate. An updated reaction rate compilation was proposed by Iliadis et al. (2010), relying on revised nuclear physics input and a Monte Carlo method for calculating the reaction rate. Later, a new precise ^{18}O(p, α)^{15}N reaction rate was presented by La Cognata et al. (2010), based on the simultaneous fit of direct measurements and of the results of a new Trojan Horse experiment. More recently, Bruno et al. (2019) obtained a revised reaction rate by integrating numerically the total cross section using their *R*-matrix fitted resonance parameters. We extracted a revised reaction rate for ^{18}O(p, α)^{15}N relying on the present fitted resonance parameters. Meanwhile, the rate of $E_r = 20$ keV resonance

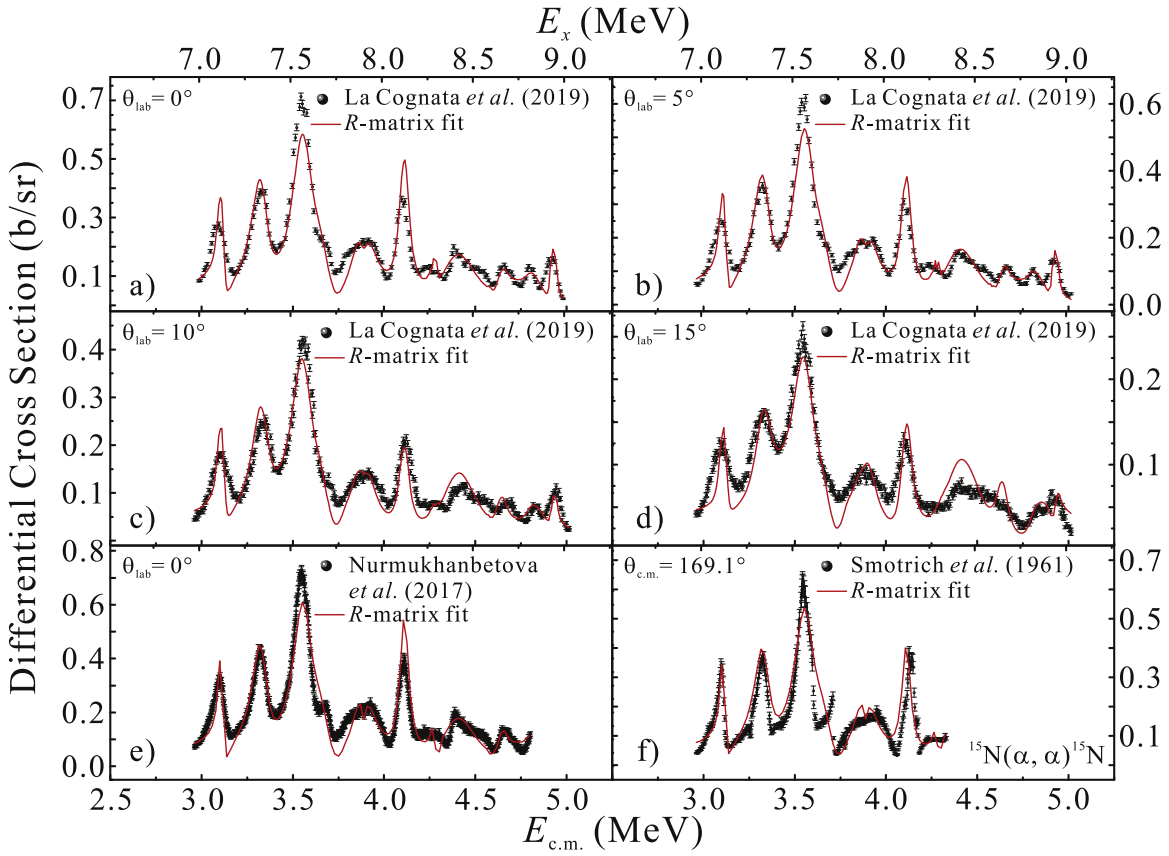

Figure 5. *R*-matrix fits to the ^{15}N(α, α)^{15}N differential cross sections of La Cognata et al. (2019) at $\theta_{lab} = 0°$, 5°, 10°, and 15°; Nurmukhanbetova et al. (2017) at $\theta_{lab} = 0°$; and Smotrich et al. (1961) at $\theta_{c.m.} = 169.°1$.

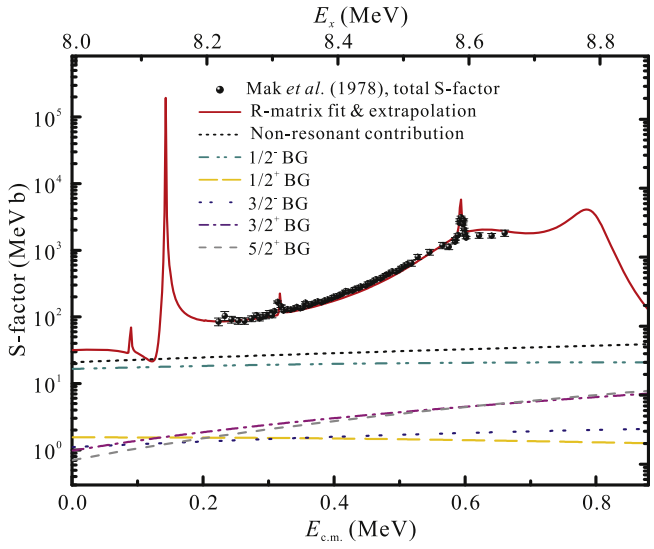

Figure 6. Extrapolation for the ^{18}O(p, α)^{15}N *S*-factor based on the present fitted level parameters.

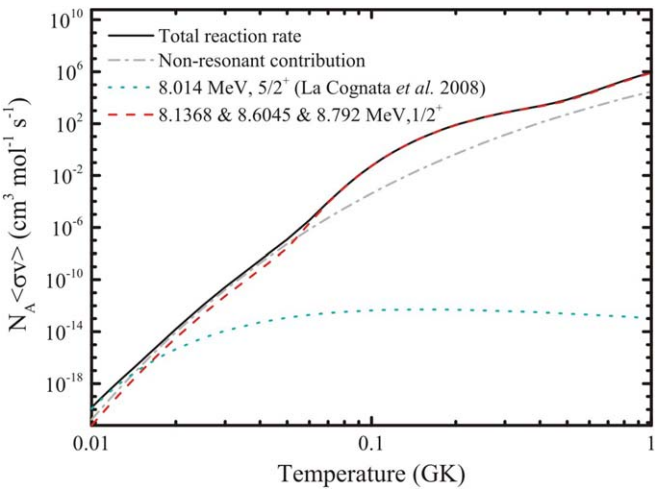

Figure 7. Ratio of the 18O(p, α)15N reaction rates to that of Iliadis et al. (2010).

was also added in the total rate following the resonance strength $\omega\gamma$ obtained by La Cognata et al. (2008).

A Monte Carlo procedure was performed to obtain the uncertainty band of reaction rate based on our errors of level parameters. A bunch of random data sets was made by changing the value of the level parameters based on their uncertainty and assuming that the underlying probability density function was Gaussian. We made 10,000 of these data sets, recalculated the reaction rate, and then plotted the distribution of the reaction rate needed to calculate at the temperatures. The lower and upper uncertainties are then defined by the 16% and 84% quantiles of the distribution.

To make a comparison, the compilation rate from Iliadis et al. (2010) is taken as a reference, to which other reaction rates are normalized. Figure 7 shows the comparison of ^{18}O(p, α)^{15}N reaction rates. The rate of this reaction is dominated by a near-threshold resonance of $E_x = 8.014$ MeV, $5/2^+$ at $T \lesssim 0.03$ GK and three interfering resonances with $J^\pi = 1/2^+$

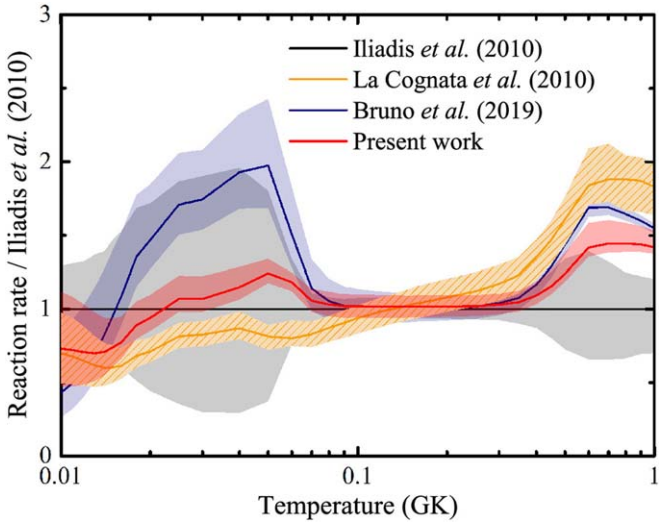

Figure 8. Comparison for the rates from the nonresonance and three interfering resonances contributions.

at $E_x = 8.1368$, 8.6045, and 8.7920 MeV at higher temperatures. The nonresonant contribution only plays an important role in the temperature region of 0.012–0.055 GK (See Figure 8). A good agreement is found within uncertainties between the present rate and that of Iliadis et al. (2010) below 0.5 GK; however, a factor of 1.5 discrepancy is presented at higher temperatures because an average of the $E_r \sim 660$ keV resonance parameters being considered in the calculations of Iliadis et al. (2010). It is obvious that our rate is lower than that of Bruno et al. (2019) and La Cognata et al. (2010) above 0.4 GK. The reason is that our $E_r \sim 660$ keV resonance parameters are the lowest values compared with theirs. A novel state of $E_x = 8.100$ MeV, $1/2^-$ was introduced in the *R*-matrix analysis of Bruno et al. (2019), and this state was also added in the rate calculation. That is why the rate of Bruno et al. (2019) is higher than both our rate and that of La Cognata et al. (2010) at 0.015–0.08 GK. A discrepancy between our rate and that of La Cognata et al. (2010) is presented around 0.05 GK. This is mainly caused by the background levels we considered and the following interference effect between resonant and nonresonant contributions. All the rates appear to be consistent within uncertainties at 0.08–0.4 GK.

5. Summary

A new global *R*-matrix analysis was performed for the ^{18}O(p, α)^{15}N reaction by involving the ^{15}N(α, α)^{15}N data for the first time. A revised determination of reaction rate was extracted, relying on the present fitting parameters. The uncertainties on the corresponding reaction rates were obtained by a Monte Carlo analysis. The present rate is generally lower than that of Bruno et al. (2019), indicating that a higher ^{18}O surface abundance would be obtained during the entire thermally pulsing AGB phase of a star with initial mass of 4.8 $M_\odot$ and solar metallicity $Z = 0.014$ (Bruno et al. 2019). This could alleviate the extent of need to assume dilution with matter of solar composition to reproduce observed abundances of most oxygen-rich Group II grains originating in intermediate-mass AGB stars.

Acknowledgments

We would like to thank R. J. deBoer and M. La Cognata for many useful discussions concerning *R*-matrix fitting. Special thanks to C. G. Bruno for providing the data of ^{18}O(p, α)^{15}N in his published PLB paper. This work was supported by the Strategic Priority Research Program of Chinese Academy of Sciences, grant No. XDB34020204, and the National Key R&D Program of China grant No. 2022YFA1603300, and the National Natural Science Foundation of China (No. 12375146).

References

Ananna, C., Barile, F., Boeltzig, A., et al. 2022, Univ, 8, 4
Azuma, R. E., Uberseder, E., Simpson, E. C., et al. 2010, PhRvC, 81, 045805
Brune, C. R. 2002, PhRvC, 66, 044611
Bruno, C., Aliotta, M., Descouvemont, P., et al. 2019, PhLB, 790, 237
Christensen, N., Jensen, F., Besenbacher, F., & Stensgaard, I. 1990, NIMPB, 51, 97
Iliadis, C., Longland, R., Champagne, A., Coc, A., & Fitzgerald, R. 2010, NuPhA, 841, 31
Jorissen, A., Smith, V., & Lambert, D. 1992, A&A, 261, 164
La Cognata, M., Fisichella, M., Di, A., et al. 2019, PhRvC, 99, 034301
La Cognata, M., Spitaleri, C., & Mukhamedzhanov, A. M. 2010, ApJ, 723, 1512
La Cognata, M., Spitaleri, C., Mukhamedzhanov, A. M., et al. 2008, PhRvL, 101, 152501
Lorenz-Wirzba, H., Schmalbrock, P., Trautvetter, H., et al. 1979, NuPhA, 313, 346
Lugaro, M., Karakas, A. I., Bruno, C. G., et al. 2017, NatAs, 1, 0027
Lugaro, M., Ugalde, C., Karakas, A. I., et al. 2004, ApJ, 615, 934
Mak, H.-B., Evans, H., Ewan, G., & Macarthur, J. 1978, NuPhA, 304, 210
Nollett, K. M., Busso, M., & Wasserburg, G. J. 2003, ApJ, 582, 1036
Nurmukhanbetova, A., Goldberg, V., Nauruzbayev, D., et al. 2017, NIMPA, 847, 125
Rolfs, C. E., & Rodney, W. S. 1988, Cauldrons in the Cosmos (Chicago, IL: Univ. Chicago Press)
Smotrich, H., Jones, K. W., McDermott, L. C., & Benenson, R. E. 1961, PhRv, 122, 232
Tilley, D., Weller, H., Cheves, C., & Chasteler, R. 1995, NuPhA, 595, 1
Yagi, K. 1962, JPSJ, 17, 604
Yagi, K., Katori, K., Ohnuma, H., Hashimoto, Y., & Nogami, Y. 1962, JPSJ, 17, 595
Zerkin, V. 2019, Experimental Nuclear Reaction Data (EXFOR), Database Version of 2024-09-17, https://www-nds.atomstandard.ru/exfor/